



UNIVERSITY OF LEEDS

This is a repository copy of *A Compression Valve for Sanitary Control of Fluid-Driven Actuators*.

White Rose Research Online URL for this paper:  
<http://eprints.whiterose.ac.uk/154538/>

Version: Accepted Version

---

**Article:**

Calò, S [orcid.org/0000-0003-4696-7498](https://orcid.org/0000-0003-4696-7498), Chandler, JH [orcid.org/0000-0001-9232-4966](https://orcid.org/0000-0001-9232-4966), Campisano, F et al. (2 more authors) (2020) A Compression Valve for Sanitary Control of Fluid-Driven Actuators. *IEEE/ASME Transactions on Mechatronics*, 25 (2). pp. 1005-1015. ISSN 1083-4435

<https://doi.org/10.1109/TMECH.2019.2960308>

---

© 2019 IEEE. Personal use of this material is permitted. Permission from IEEE must be obtained for all other uses, in any current or future media, including reprinting/republishing this material for advertising or promotional purposes, creating new collective works, for resale or redistribution to servers or lists, or reuse of any copyrighted component of this work in other works. Uploaded in accordance with the publisher's self-archiving policy.

**Reuse**

Items deposited in White Rose Research Online are protected by copyright, with all rights reserved unless indicated otherwise. They may be downloaded and/or printed for private study, or other acts as permitted by national copyright laws. The publisher or other rights holders may allow further reproduction and re-use of the full text version. This is indicated by the licence information on the White Rose Research Online record for the item.

**Takedown**

If you consider content in White Rose Research Online to be in breach of UK law, please notify us by emailing [eprints@whiterose.ac.uk](mailto:eprints@whiterose.ac.uk) including the URL of the record and the reason for the withdrawal request.



[eprints@whiterose.ac.uk](mailto:eprints@whiterose.ac.uk)  
<https://eprints.whiterose.ac.uk/>

# A Compression Valve for Sanitary Control of Fluid Driven Actuators

Simone Calò, *Student Member, IEEE*, James H. Chandler, *Member, IEEE*, Federico Campisano, *Student Member, IEEE*, Keith L. Obstein and Pietro Valdastrì, *Senior Member, IEEE*

**Abstract**—With significant research focused on integrating robotics into medical devices, sanitary control of pressurized fluids in a precise, accurate and customizable way is highly desirable. Current sanitary flow control methods include pinch valves which clamp the pressure line locally to restrict fluid flow; resulting in damage and variable flow characteristics over time. This paper presents a sanitary compression valve based on an eccentric clamping mechanism. The proposed valve distributes clamping forces over a larger area, thereby reducing the plastic deformation and associated influence on flow characteristic. Using the proposed valve, significant reductions in plastic deformation (up to 96%) and flow-rate error (up to 98%) were found, when compared with a standard pinch valve. Additionally, an optimization strategy presents a method for improving linearity and resolution over the working range to suit specific control applications. The valve efficacy has been evaluated through controlled testing of a water jet propelled low-cost endoscopic device. In this case, use of the optimized valve shows a reduction in the average orientation error and its variation, resulting in smoother movement of the endoscopic tip when compared to alternative wet and dry valve solutions. The presented valve offers a customizable solution for sanitary control of fluid driven actuators.

**Index Terms**—Hydraulic/Pneumatic actuation, medical robotics, soft robotics, waterjet actuation.

## I. INTRODUCTION

THE concepts of precision and accuracy are central in the field of robotics. The ability of a robot to generate reproducible and exact motions depends on the performance of its actuators; whether electromechanical, pneumatic or hydraulic in nature. In these latter cases, precise introduction of pressurized fluid is fundamental in facilitating reliable high resolution actuator control for many applications. For example, soft robotic systems based on the construct of pressure

Research reported in this article was supported by the Royal Society, by the Engineering and Physical Sciences Research Council (EPSRC) under grant number EP/P027938/1, by the National Institute of Biomedical Imaging and Bioengineering of the National Institute of Health under Award Number R01EB018992, by the National Institute for Health Research (NIHR) (16/137/44) using UK aid from the UK Government to support global health research, and by the European Research Council (ERC) under the European Union's Horizon 2020 research and innovation programme (grant agreement No 818045). Any opinions, findings and conclusions, or recommendations expressed in this article are those of the authors and do not necessarily reflect the views of the Royal Society, EPSRC, NIH, NIHR, the UK Department of Health and Social Care or the ERC.

S. Calò, J. H. Chandler and P. Valdastrì are with the STORM Lab UK (Science and Technology of Robotics in Medicine), School of Electronic and Electrical Engineering, University of Leeds, LS2 9JT, Leeds, UK. Corresponding author's e-mail: (s.calol@leeds.ac.uk).

F. Campisano and Keith L. Obstein are with the STORM Lab USA (Science and Technology of Robotics in Medicine), Department of Mechanical Engineering, Vanderbilt University, Nashville, TN, USA

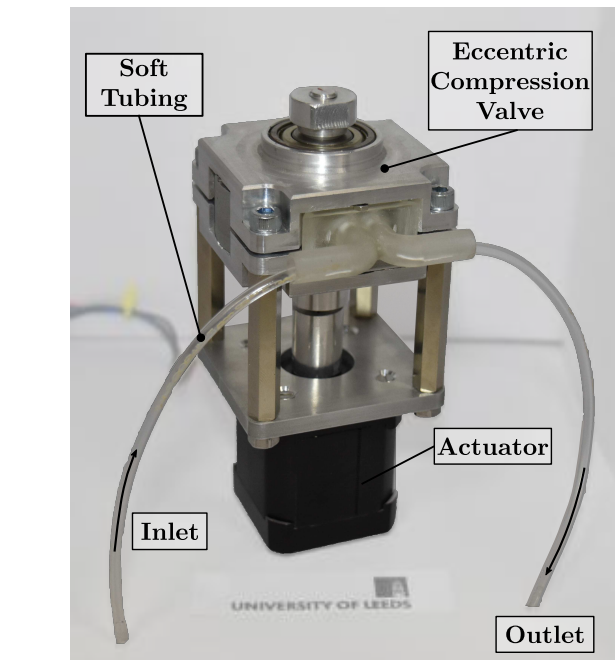


Figure 1. Assembled eccentric compression valve showing the sanitary valve inlet and outlet, the soft tubing, the valve core and actuator.

driven hyper-elastic materials (e.g. silicone) generate a kinetic response that depends directly on fluid control coupled with the robot's geometry and material properties [1]. Research into soft robot based applications for augmenting the capabilities of traditional robots [2] and for environmental exploration [3], [4], [5] is common, however, one of the most prevalent areas of interest for soft robotics is within medical applications [6]. Devices have been developed for Minimally Invasive Surgery (MIS) [7], endoscopy [8], heart assistance [9] and rehabilitation [10].

For medical use cases, such as those exemplified, consideration of patient safety during interaction with the device materials and drive system is crucial. Although regulation of fluids through in-line valve systems (e.g. gate valves, needle valves, etc) can offer technically effective solutions, they require direct interaction with the working fluid. This adds to contamination risks either from the valve directly (i.e. corrosion), or cross-contamination of patients (i.e. back-flow). Therefore, such in-line systems must be disposable or be subject to reprocessing protocols that increase the cost and downtime of the device [11].

Pressure or flow regulation devices that are physically

separate from the transmission fluid offer a more appropriate solution for medical applications. Examples include pinch valves [12], [13] and peristaltic pumps [14] used for sanitary applications such as dosage regulation and blood analysis or infusion. Pinch valves work by applying a load normally to pre-pressurized tubing through a “pinch-point” plunger; thus reducing the cross-sectional area of the tube locally and consequently the flow-rate. This flow regulation approach generates a high level of stress on the soft tubing leading damage and ultimately altering the flow characteristics of the system over time [14]. Peristaltic pumps induce pressure in the line through successive simultaneous squeezing and shearing actions. In this case, the output flow generated by the pump is highly pulsatile, which is undesirable if a fine control of the pressure/flow needs to be achieved. This behaviour can be attenuated by introducing an inline pulsation damper [15], although this adds complexity and cost to the system. These issues, when coupled with poor resolution in flow-rate control and hysteresis, make them unsuitable for applications such as medical actuators that require great precision. Therefore, there is a need for sanitary pressure and flow regulation devices that deliver safe and precise flow control.

This paper presents a novel sanitary eccentric compression valve (ECV) that allows indirect precise flow regulation in pre-pressurized systems. The ECV, presented in Figure 1, uses an eccentric mechanism to compress the tubing over a wider contact area against a tunable spiral shaped profile, thereby minimizing local stresses and the associated tube damage. An optimization step is presented that allows for the geometry of the device to be easily adapted to suit the components and constraints of a wide range of applications. The method applies to the mechanical design of the valve rather than on its electronic controller to produce improved resolution and linearity with respect to commercially available sanitary solutions.

The presented work evaluates our novel ECV performance against standard pinch valves in terms of volumetric flow-rate characteristics over repeated actuation cycles. For the purpose of this manuscript, the valve efficacy was demonstrated by using an optimized ECV to control the medical device known as the *HydroJet*: a portable water jet actuated capsule endoscope [8], [16]. Comparison of the ECV relative to pinch and solenoid valves under cyclic actuation of the *HydroJet* is presented and highlights improved flow-rate tracking and reduced flow-rate fluctuation.

## II. PRINCIPLE OF OPERATION

The proposed valve adopts a combination of custom components to deliver a gradually increasing distributed load onto standard flexible tubing carrying a pressurized fluid. The design is comprised of two main parts, as shown in Figure 2a: (1) a passive compression component (valve housing) that includes a spiral compression profile encoded into its wall; and (2) an active compression component with eccentric geometry (eccentric drive shaft and compression bearing). Flexible tubing sits between these two components and is compressed between the bearing and the compression profile. Through

the use of a bearing, shear forces induced by the relative motion between the rotating drive shaft and the flexible tube are minimized ensuring compressive forces remain normal to the tubing cross-section. Relative motion between the active and passive components therefore, results in varied occlusion of the flexible tubing and hence alters the volumetric flow-rate of the fluid (Figure 2b). The level of compression depends on the rotation angle of the rotary actuator shaft with respect to the tube housing. In the general case, the compression profile radius  $r$  may be expressed as a function of an angle  $\theta$ , evaluated across an angular range,  $\theta_i$  to  $\theta_e$ , as:

$$r = r(\theta) \quad \{\theta \mid \theta_i \leq \theta \leq \theta_e\} \quad (1)$$

The choice of  $r(\theta)$  and tube size are application dependent, and may be interchanged while maintaining the same active compression components. For the example case presented in Figure 2, an Archimedean spiral of the form  $r = r_i + k\theta$  has been used to generate a linearly varying compression profile as a function of angular position, where  $r_i$  and  $k$  represent the initial compression radius and its angular rate of variation, respectively.

The spiral parameters  $r_i$  and  $k$  can be evaluated by considering the bearing eccentricity ( $c$ ), the bearing radius ( $b$ ), the geometry of the flexible tubing (e.g. tube inner diameter ( $id$ ) and wall thickness ( $wt$ )), and the working angular range ( $\theta_e - \theta_i$ ); allowing for suitable tubing access into and out of the housing.

With a desired profile selected, the components of the valve may be assembled from a combination of off-the-shelf components (e.g. ball bearings and drive motor), machined parts (e.g. upper and lower casing, tube housing, drive shaft, etc), and parts produced with additive manufacturing (e.g. tube feeder and tube guide), as illustrated in Figure 3. This approach delivers a flexible design for accommodating different application requirements, for example: tube sizing, machining resolution, drive torque, actuation speed, and positional resolution.

In addition to being scalable to different applications, the mechanical design of the valve intrinsically limits the maximum stress that can be applied on the flexible tube since the gap between active and passive pinching components is fixed, never falling below a pre-designed threshold. This will increase the longevity of the tubing and reduce the influence of damage on the output flow characteristics. As an example, a minimum closing threshold equal to twice the wall thickness ( $wt$ ), and a maximum exactly equal to the thickness of the uncompressed tubing with outer diameter ( $id + 2wt$ ) may be used as design inputs to minimize excessive stress on the tubing while maintaining high compression resolution (Figure 2b).

Implementation of a continuously variable compression profile allows for valve customization to match the flow characteristic of a specific pressure-tubing configuration or application. The level of customization is thereby only limited by the manufacturing process used to produce the valve. Through experimental assessment of the relationship between flow-rate (or output pressure or force) and tube occlusion, the

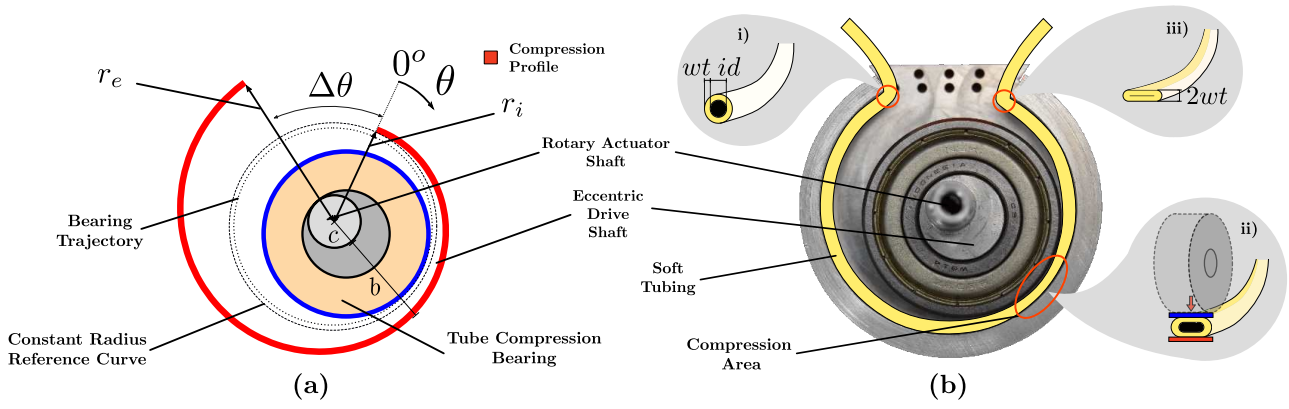


Figure 2. Example compression profile: showing (a) a design with a linearly varying compression profile (exaggerated for clarity), and (b) a schematic representation of tube compression at three locations along the profile, with: i) no occlusion - maximum flow, (ii) moderate occlusion - intermediate flow, and (iii) completely occluded - no flow.

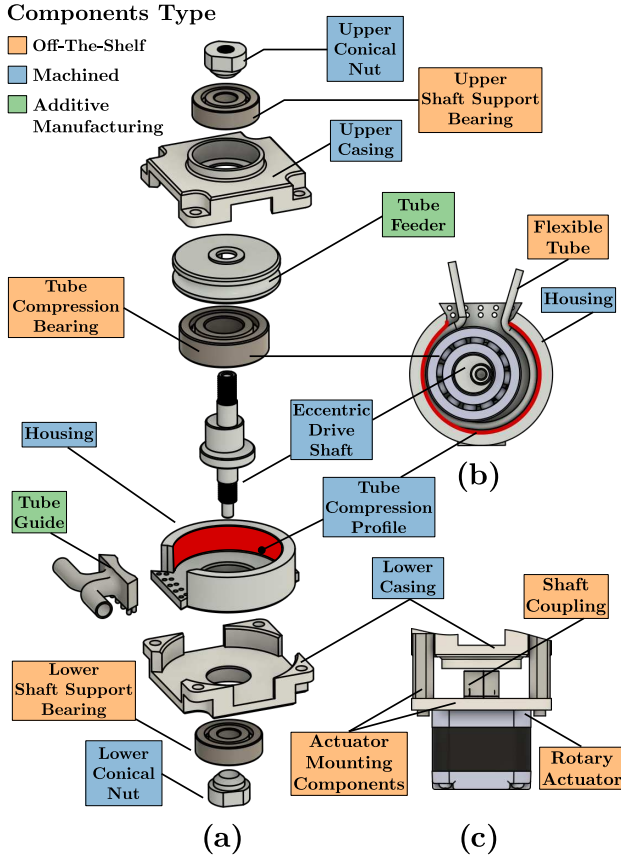


Figure 3. Sanitary ECV design, showing: (a) exploded view of the valve housing assembly; (b) the active and passive components acting to compress the tubing; and (c) the rotary actuator and its coupling to the housing assembly.

profile may be optimized to deliver any desired response with shaft angle across the desired working range. An example optimization scheme, for generating a linearly varying flow-rate output, has been presented in Section III-A.

### III. VALVE DESIGN, OPTIMIZATION AND MANUFACTURING

An initial valve design was implemented using an Archimedean (linearly varying radius) spiral as described previously. Further practical considerations made to determine the shape of the compression profile were:

- A suitable opening  $\Delta\theta$  (Figure 2a) in the housing should be included that is wide enough to accommodate the tubing and avoid undesired tubing compression when the valve is completely open.
- When the valve is in the completely closed position, the tube should be totally occluded.
- When the valve is in the completely open position, no occlusion should be present on the tube.

To evaluate the radius of the profile under the completely closed position (i.e.  $r(\theta_i) = r_i$ ), the bearing radius  $b$ , the distance between the shaft and the bearing's centers (bearing eccentricity)  $c$ , and the tube wall thickness  $wt$  were considered in accordance with:

$$r_i = b + c + (2 \cdot wt) \quad (2)$$

That is, the completely closed state is assumed to occur when the space between the bearing and housing is equal to twice the tube wall thickness. Similarly, the maximum radius  $r_e$  was calculated to occur at the maximum angle (i.e.  $r(\theta_e) = r_e$ ), and to generate a spacing exactly equal to the thickness of the uncompressed tubing as:

$$r_e = r_i + id \quad (3)$$

Considering that, in the implemented design, the profile starts at  $\theta = \theta_i$  and stops at  $\theta = \theta_e$ , and that it varies linearly with the angle  $\theta$ , it can be described parametrically in Cartesian coordinates using:

$$r(\theta) = \left( \frac{r_e - r_i}{\theta_e - \theta_i} \cdot \theta - \frac{\theta_e \cdot r_i - \theta_i \cdot r_e}{\theta_e - \theta_i} \right) \quad (4a)$$

$$x(\theta) = r(\theta) \cdot \sin(\theta) \quad (4b)$$

$$y(\theta) = r(\theta) \cdot \cos(\theta) \quad (4c)$$

### A. Output Optimization

For the purpose of optimizing the compression profile to match the needs of a particular application in terms of flow-rate resolution and linearity, (1) was adjusted to account for the non-linear response of tube compression vs flow-rate.

Optimization was performed using flow-rate vs position data collected using the linearly varying profile ECV. A representative function  $g(r, \sigma)$  was selected and fit to these data using a curve fitting algorithm to evaluate the set of function parameters  $\sigma$ . Subsequently, a minimization process was performed to evaluate the compression profile shape required to linearize the output flow-rate vs position characteristic. A desired optimized compression profile curve function  $\hat{r}(\theta, \lambda)$ , where  $\lambda$  is an unknown set of function parameters, will cause a transformation of the output profile  $g(r, \sigma)$  to a straight line  $g(\hat{r}, \sigma)$  passing through the origin and the point where the output is maximum. Formulating this problem as in (5a) allows the coefficients  $\lambda$  of the optimized compression curve function  $\hat{r}(\theta, \lambda)$  to be iteratively updated to minimize the difference between  $g(r, \sigma)$  and  $g(\hat{r}, \sigma)$ :

$$\min_{\lambda} \sum_{j=1}^n w_j \cdot (g(r(\theta_j), \sigma) - g(\hat{r}(\theta_j, \lambda), \sigma))^2 \quad (5a)$$

$$x(\theta) = \hat{r}(\theta, \lambda) \cdot \sin(\theta) \quad (5b)$$

$$y(\theta) = \hat{r}(\theta, \lambda) \cdot \cos(\theta) \quad (5c)$$

where  $w$  represents the weightings used to constrain the evaluation of  $\hat{r}(\theta, \lambda)$  to obtain a  $g(\hat{r}(\theta, \lambda))$  that starts at 0 and ends at the maximum output. The optimization process eventually produces the set of parameters  $\lambda$  and then (5b) and (5c) as a result.

The curve fitting on experimental data was performed using a function of the form:

$$g(r(\theta), \sigma) = \frac{a_1}{\pi} \cdot \left( \arctan(b_1 \cdot r + c_1) + \frac{\pi}{2} \right) + d_1 \quad (6a)$$

$$\sigma = (a_1 \ b_1 \ c_1 \ d_1) \quad (6b)$$

Finally, an  $\hat{r}(\theta, \lambda)$  with unknown parameters  $\lambda$ , in the form:

$$\hat{r}(\theta, \lambda) = -\frac{a_2}{b_2} - \left( \frac{1}{b_2} \cdot \tan \left( (c_2 - \theta) \cdot \frac{\pi}{d_2} + \frac{\pi}{2} \right) \right) \quad (7a)$$

$$\lambda = (a_2 \ b_2 \ c_2 \ d_2) \quad (7b)$$

was used to evaluate the compression profile shape. The linearly varying compression profile  $r(\theta)$ , and the resulting optimized compression profile  $\hat{r}(\theta, \lambda)$  are shown in Figure 4a. Expected flow-rate characteristics for the two compression profiles are shown in Figure 4b. It is worth mentioning that in an ideal case the optimization result (expected flow-rate output) and the desired output would coincide. Instead, in the real case, the minimization problem stops when a minimum of the error function (5a) is detected thus introducing a disparity between the two curves.

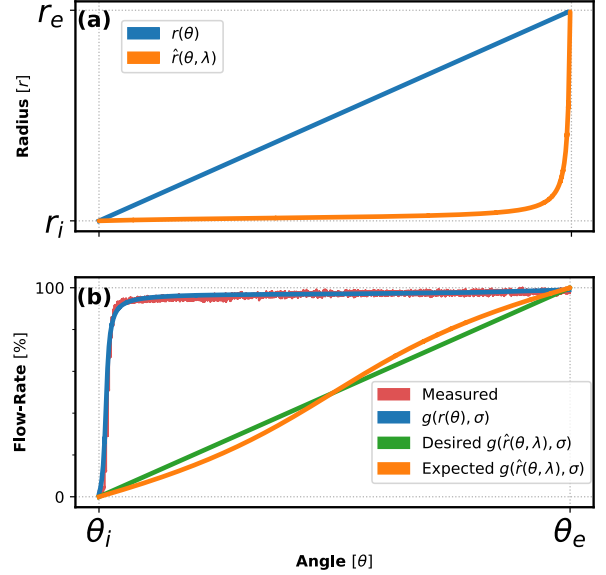


Figure 4. (a) Compression radius vs angle relationship for linearly varying and optimized compression profiles. (b) Volumetric flow-rate characteristic measured using a linearly varying compression profile, curve fitting, desired and expected optimization output.

### B. Device Manufacturing

Two valve designs were fabricated to deliver a linearly varying compression profile ( $r(\theta)$ ), and the optimized compression profile ( $\hat{r}(\theta, \lambda)$ ), respectively. The design parameters used to fabricate the two ECV for use with 1/8" inch diameter tubing are summarized in Table I.

Table I  
DESIGN PARAMETERS IMPLEMENTED FOR A LINEARLY VARYING PROFILE ECV DESIGN FOR 1/8" INCH OD TUBING.

Parameter	Value
$r_i$	24.6 mm
$r_e$	26.4 mm
$c$	3.2 mm
$b$	20.0 mm
$wt$	0.79375 mm
$id$	1.5875 mm
$\Delta\theta$	60.0°
$\theta_i$	0°
$\theta_e$	300°

As the width of the gap between active and passive compression components is responsible for fine tuning the flow-rate, a number of additional parts were integrated to ensure accurate and precise alignment (Figure 3). Firstly, the upper and lower casings are equipped with ball bearings to align the tube housing with the eccentric drive shaft. To further promote concentric placement, both ends of the shaft are secured to the bearings using two conical aligning nuts. Secondly, to make sure the flexible tube is always in an optimal position in the housing and to reduce its vertical displacement, a tube feeder and a guide are also included.



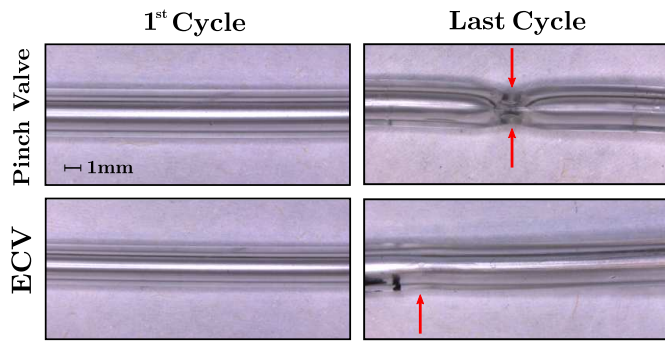


Figure 6. Visual influence of repeated valve actuation on 70 Shore A tubing; showing microscope images of actuation locations before and after 3000 cycle tests. Red arrows highlight the identified points of maximum stress.

avoid potential error produced by missed steps. Similarly, to ensure position-flow repeatability for the ECV, a 600 pulse-per-revolution absolute encoder (04A23902, British Encoder Company, UK) was coupled to the shaft and used to monitor the absolute shaft position and to identify possible missed steps.

After each test, the tube was removed and the visible level of plastic deformation assessed using a microscope (DMS300, Leica, Germany). Objective measures of tube damage (% reduction in diameter) were determined through comparison of the undeformed tubing thickness to the region of minimum tube thickness; measured at tubing regions that were outside and inside of the valve mechanism respectively. Thickness values were determined through calibrated software measurement, using a known length reference and image analysis software (LAZ EZ, Leica, Germany).

To evaluate the variation in position-flow characteristics for each durometer-valve combination, comparison was made between the first cycle response and subsequent cycles. To quantify relative error, the difference between the flow-rate at the position of 50% maximum flow on the first cycle and the flow-rate at the same position on the n-th cycle was determined. These data were calculated for each measured cycle and normalized to their respective cycle 1 maximum flow. At a pressure difference of 30 PSI, the maximum registered flow-rate was 0.324 l/min, corresponding to the valves in a completely open state.

1) *Visual Assessment*: Following the cyclic operation of the dry valves, each tube durometer-valve combination was analyzed to determine the level of plastic deformation present. An example comparison of the level of visible damage on the 70 Shore A hardness tubing before use and after 3000 actuation cycles using the pinch valve and ECV is shown in Figure 6. Objective measures of tube damage (% reduction in diameter) for all durometers are presented in Table II. It is evident from Figure 6 that the pinch valve induces greater visible plastic deformation on tubing when compared to the ECV. This finding is consistent across durometers, with the average (mean  $\pm$  SD) percentage reduction in tube diameter across all durometers being  $21.6 \pm 13.8\%$  and  $2.7 \pm 2.3\%$  for the pinch valve and ECV, respectively, which is statistically significant ( $p < 0.05$ ) under a Student's t-test.

Table II  
TUBE DAMAGE INDUCED BY REPEAT VALVE ACTUATION ON DIFFERENT TUBE DUROMETERS; SHOWING RESIDUAL % REDUCTION IN DIAMETER MEASURED AFTER 3000 CYCLES.

	Durometer					
	40 A	50 A	55 A	60 A	65 A	70 A
Pinch valve	-	3.0	14.1	21.5	31.7	37.7
ECV	-	1.7	1.0	0.9	3.6	6.4

'-' represents no visually identifiable change in tubing diameter.

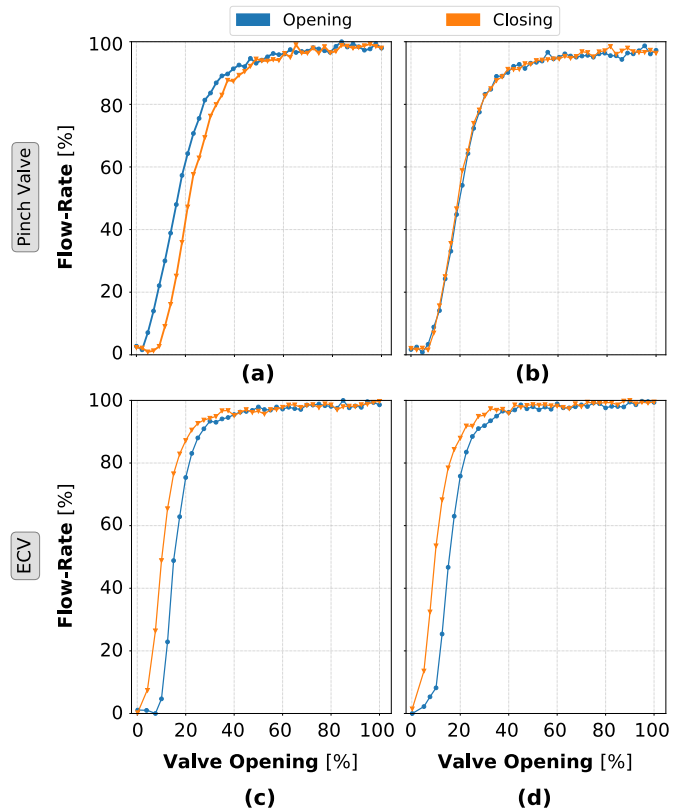


Figure 7. Influence of repeat valve actuation on the hysteretic behaviour of the sanitary valves. Graphs a) and c) show the hysteresis loop during the first actuation cycle. Graphs b) and d) refer to the last (3000<sup>th</sup>) cycle.

2) *Flow Characteristic Variation*: Example opening and closing flow-rate responses for the pinch valve and ECV at the first and last test cycle are shown in Figure 7. With fresh tubing (Figure 7a and 7c), the valve position vs flow-rate characteristic includes a hysteretic behaviour for both the pinch valve and the ECV. After 3000 loading cycles, the level of hysteresis for the pinch valve is reduced while the ECV response remains broadly unchanged, as shown in Figure 7b and 7d respectively.

Figure 8 presents the relative error in the 50% of maximum flow-rate position as a function of loading cycle for each durometer-valve combination for opening and closing. The graph highlights that, when using the pinch valve (Figure 8a to 8c), the relative error drifts significantly as the number of cycles increases; prevalent across all tubing durometers for opening and closing procedures. When coupled with low

Table III  
PERCENTAGE SHIFT IN 50% MAXIMUM FLOW-RATE POSITION BETWEEN  
CYCLE 1 AND CYCLE 3000.

		Durometer					
		40 A	50 A	55 A	60 A	65 A	70 A
<b>Pinch valve</b>		23.5	33.5	43.6	33.7	27.6	11.7
<b>ECV</b>		11.7	11.4	5.2	1.9	0.5	2.3

durometer tubing (40A-55A), the pinch valve shows less variability (Figure 8b), however, the median error remains high; particularly for the opening procedure. Conversely, for the ECV the reduced variability is coupled with low overall median error for opening and closing procedures (Figure 8e). Table III summarizes the relative error through comparison of the 3000th cycle for each valve-durometer combination. The average (mean  $\pm$  SD) percentage shift across all durometers was  $28.9 \pm 10.8\%$  and  $5.5 \pm 4.9\%$  for the pinch valve and ECV respectively, which was statistically significant ( $p < 0.05$ ) under a Student's t-test.

### B. Valves Comparison

In addition to evaluating the level and influence of plastic deformation in dry valve tubing, the ECV with a linearly varying compression profile was also compared with its optimized equivalent and a wet valve alternative (in-line solenoid valve). Each valve was tested using the same experimental setup as for cyclic loading tests (Figure 5) over 10 repeats at a cycle actuation rate of 5 steps-per-second while position and flow-rate data were recorded.

The volumetric flow-rate characteristics as a function of valve position for the linearly varying and optimized ECV designs are shown in Figure 9. For comparison, the desired and expected position vs flow-rate linear response of the optimized ECV are also presented.

The linearly varying ECV demonstrates a non-linear relationship between flow and position which leads to poor flow-rate resolution of the valve within the working range. This results in 90% of the maximum flow-rate being reached within the first 16.2 degrees (equivalent to 18 steps), while the remaining 263.7 degrees (293 steps) are used to control only the final 10% of the flow-rate range. The optimized ECV profile instead shows a response with more even flow-rate changes across the entire position range. Measured data from the optimized profile ECV, however, differs from the expected output and maintains a significant level of hysteresis.

Figure 10 makes direct comparison of the valve position vs flow-rate response for the four valves: pinch valve, solenoid valve, linearly varying and optimized ECV. The poor resolution of pinch and solenoid valve is evident, with the flow-rate saturating after 50% of the respective valve ranges. The dynamic influence of the step resolution is also clear; as large flow-rate jumps are recognizable throughout the working range. Conversely, the optimized profile ECV maintains a smooth increasing flow-rate across the full range of valve

positions, however, demonstrates a similar level of variability to the pinch valve across 10 repeats.

## V. CASE STUDY - THE HYDROJET

With improved linearity and resolution (Figure 10), and reduced variation in valve position vs flow-rate characteristics under repeated actuation (Figure 8), it is important to understand the impact of using an optimized ECV on the controllability of an application-specific actuator. To this end, this section demonstrates the optimized ECV applied to a flow-rate controlled soft manipulator. Example designs were fabricated to suit the HydroJet endoscopic capsule device.

### A. The HydroJet Platform

The HydroJet system [16], [17], [8], shown in Figure 11, consists primarily of a disposable capsule attached to the end of a soft multi-lumen catheter, which is used to carry pressurized water from the control system to the capsule. The flow-rate of the three pressure lines has previously been controlled independently through electronic actuation of a line-specific pinch valves (*MPPV-2*, Resolution Air, USA), [8]. As illustrated in Figure 11, three nozzles, placed on the capsule's body at an even  $120^\circ$  spacing, facilitate ejection of pressurized water; thereby inducing movement in the capsule as a result of the generated jet thrust  $T$

$$T = \rho \cdot \dot{V}^2 \cdot \left( \frac{1}{A_{out}} - \frac{1}{A_{in}} \right) \quad (8)$$

where  $\rho$  is the density of water,  $\dot{V}$  is the volumetric flow-rate,  $A_{in}$  and  $A_{out}$  are geometric parameters of the nozzles, inlet and outlet sections respectively.

Due to the soft and flexible nature of the device, even modest fluctuations in flow-rate can lead to significant position and orientation variation. This therefore, precludes the implementation of autonomous or semi-autonomous control strategies, and increases the demand on the operator. The optimized ECV design was therefore evaluated within the context of the HydroJet application, under direct comparison to pinch and solenoid valves. However, the design methodology and assessment techniques presented may be extended to any device requiring the sanitary control of fluid flow.

Alongside repeatability, flow-rate resolution is also crucial in the actuation of the HydroJet system. The possibility to fine tune the flow-rate, and consequently the jet thrusts, allows for smooth trajectories between desired positions and delivers stable anatomy visualization during a gastroscopy procedure.

To test the influence of the three valves on the performance of the HydroJet, a single jet bending test was performed by controlling its flow-rate (see the video in the multimedia extension). Sinusoidal command profiles at different frequencies were selected to simulate open-loop valve control. For each valve, a sinusoidal command with a fixed frequency of either 0.05 Hz, 0.1 Hz or 0.2 Hz was supplied to its controller while the flow-rate and tip pose were measured using an ultrasonic flowmeter (see Section IV) and magnetic tracker (*Aurora Electromagnetic Tracking System*, NDI), respectively. Each valve-frequency combination was tested over 10 cycles.

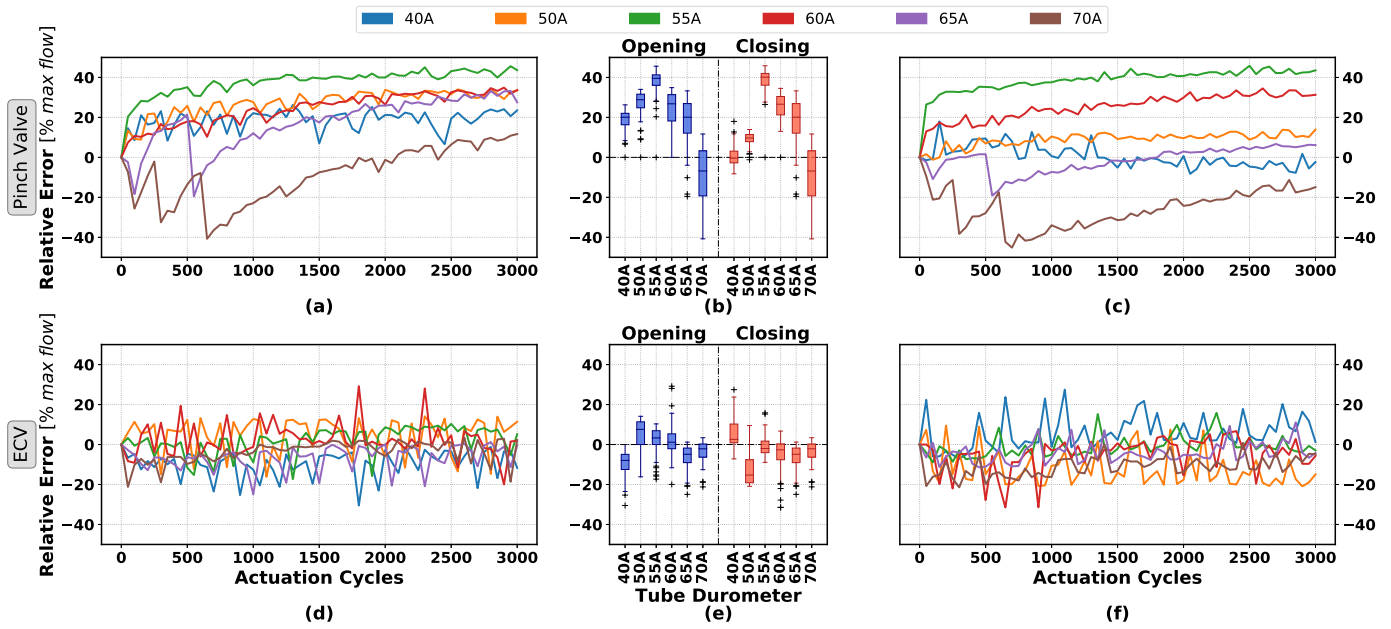


Figure 8. Flow-rate error (evaluated as the difference between the flow-rate at the position of 50% maximum flow on the first cycle and the value of the flow-rate at the same position on the n-th cycle) for varied durometers over 3000 actuation cycles; showing: pinch valve opening (a), closing (c), ECV opening (d), closing (f). Median and inter-quartile range, referring to opening and closing for the pinch valve (b) and ECV (e).

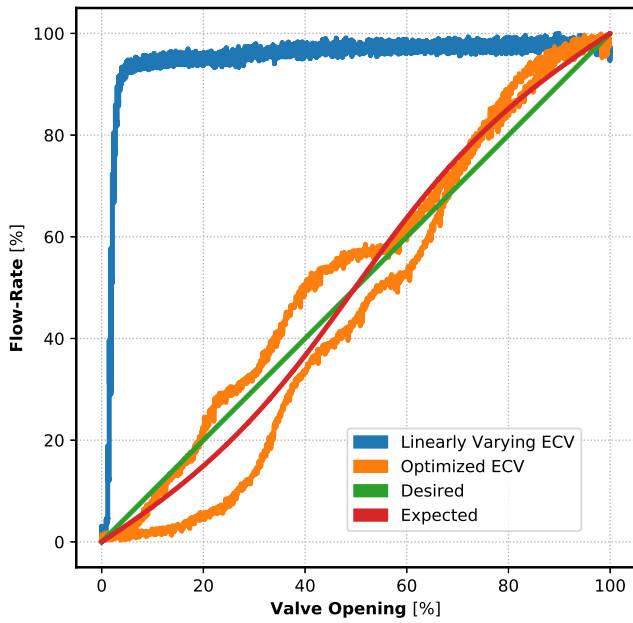


Figure 9. Flow-rate characteristics of the ECV generated by a linearly varying compression profile (blue) and using the optimized profile (orange). The desired response used for optimization (green) and the expected output based on the optimized profile attained (red) are also shown.

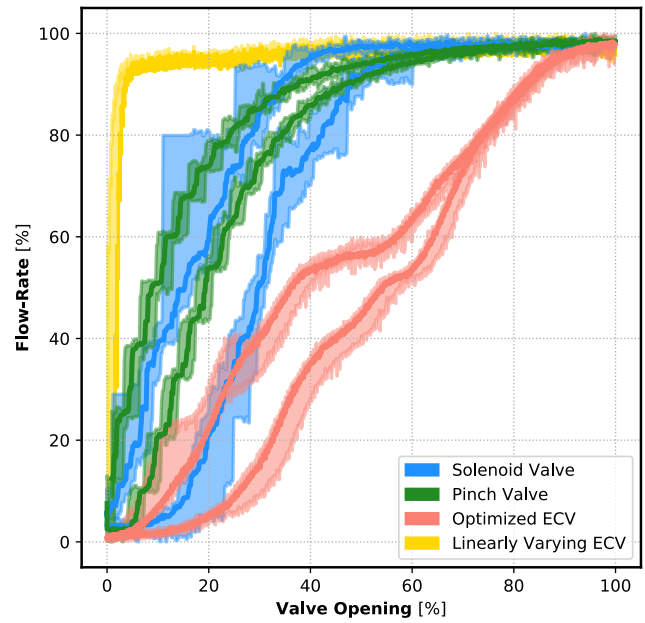


Figure 10. Volumetric flow-rate characteristics generated by the solenoid valve (blue), pinch valve (green) and ECV (red), linearly varying ECV (yellow), evaluated as the median (dark curves), maximum and minimum values (shaded area) over 10 repetitions for both opening and closing procedures.

Figure 12a shows the tip angle response over two cycles at each frequency for the three valves.

The desired bending angle was evaluated starting from the sinusoidal command fed to the valve and the assumption of quadratic relation between volumetric flow-rate and bending angle. Then, the valve command was re-scaled in the range

between  $0^\circ$  and the maximum bending angle achieved for the valve under test (approximately  $70^\circ$ ) when the flow-rate is maximum.

The ECV output shows smoother tip movements across all frequencies when compared to the solenoid and pinch valve. Overall, the ECV allows the tip to follow the desired pattern

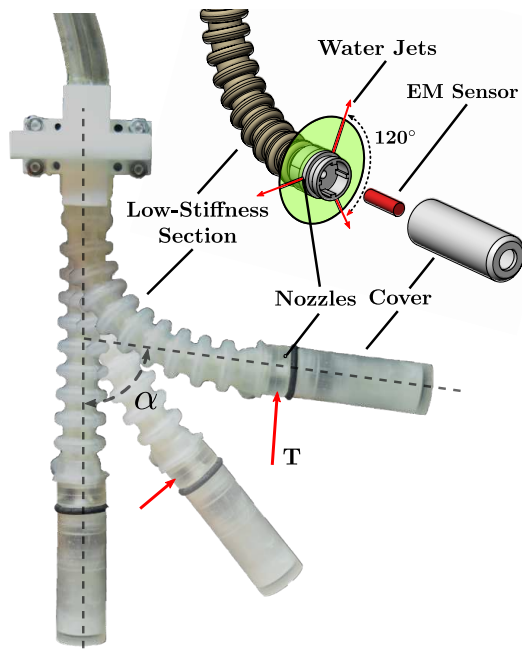


Figure 11. The HydroJet System consisting of a disposable capsule (nozzles unit and cover) that contains an electromagnetic sensor. The low-stiffness of the tether allows the capsule to move as a result of the thrust (T) generated by the water jets.

with higher accuracy for all the applied commands (median errors 5.3%, 3.1% and 4.8% for the three proposed signal frequencies), as shown in Figure 12b. Comparative median errors are significantly higher for the pinch valve (32.5%, 29.7% and 33.6%) and solenoid valve (16.2%, 15.6% and 17.5%) respectively.

The magnitude of the flow-rate variation, and consequently the change in bending angle, resulting from opening or closing the valve one step at a time, is presented in Figure 13a. For solenoid and pinch valve, approximately 75% of the fluctuations stay below 5% of flow-rate variation; however more extreme values are present and reach maxima of 19.2% and 14.2%, respectively. Conversely, the ECV shows flow-rate variations generally smaller than 1%, with extreme values remaining under 4%. The effect of these flow-rate variations on the jet thrust produced and therefore on the capsule bending angles ( $\alpha$ ) is shown in Figure 13b. In the supplementary video, the amplitude of the oscillatory movement of the HydroJet capsule is presented for each valve; using a contour plot to locate the oscillations along the capsule trajectory. Congruently with the previous results, the smoother flow-rate profile produced by the ECV translate into higher actuation accuracy and an absence of oscillations.

## VI. DISCUSSION

The reduced plastic deformation (Figure 6) and change in position vs flow-rate characteristics after repeated operation (Figure 7) realized by the ECV represent improved open-loop performance relative to the pinch valve. Although significant hysteresis is present in the flow characteristic, this is largely invariant with cyclic operation and may therefore be accounted for with an appropriate valve model. In contrast, the pinch

valve shows a reducing but varying level of hysteresis, which amplifies complexity in generating a suitable valve model.

The reduced levels of plastic deformation were realized through increased contact area between the tubing and valve housing and the moving compression point, intrinsic to the ECV design. Although improvements may be possible with modification to the pinch valve contact area, it is not feasible to introduce a moving contact point within its existing design.

Tubing durometer has also been shown to influence flow characteristics during cyclic operation (Figure 8). Using the pinch valve shows larger drift across the cycle range tested when compared to the ECV, as summarized in Table III. These characteristics make selection of a suitable tube durometer for the valves challenging, particularly for the pinch valve. However, with consideration of both precision and accuracy, the results indicate that a tube durometer of 55A is most suitable for use with the ECV while 50A is least suitable.

With reduced flow-rate drift, it becomes feasible to use the valve for applications requiring a varying test duration. In the presented study, a duration of 3000 cycles was selected in relation to the case study described in Section V. This was chosen considering two factors: the maximum speed at which the ECV can be operated and an estimation of the time of completion for a gastroscopy procedure. Given that the current maximum speed without motor stall is 1000 steps/s (from completely closed to completely open in 0.333s) and a worst-case scenario gastroscopy procedural time of 30 minutes [18], the ECV will be able to perform a maximum of  $\approx 2700$ , approximated to 3000, cycles during each procedure.

Through optimization of the ECV design (Subsection IV-B), a more linear flow-rate response with improved resolution was produced, as shown in Figure 10. Although effective, the optimized ECV still shows error with respect to the desired profile. Factors that are likely to contribute to this are: accuracy and precision of the manufacturing process used to generate the profile, profile-tubing alignment, imperfect fitting of measured data used for the optimization process and changes in the flow-rate regime which have not been considered in this work. For applications requiring even higher levels of flow control precision, these factors may be improved incrementally.

For the presented case study in Section V, implementing the optimized ECV shows reduced variation in flow-rate and bending angle error (Figure 13). This results from the improved linearity and resolution of the ECV with respect to the solenoid and pinch valves; which show abrupt changes in flow-rate during opening and closing (Figure 10). In the supplementary video, these differences may be seen in terms of oscillatory movement of the HydroJet tip. Although this is one specific test case, achieving improved performance in open-loop sanitary flow control may be beneficial to a wide range of future applications, particularly in the field of soft medical robotics.

## VII. CONCLUSIONS

A novel design methodology for a sanitary fluid flow control system has been presented and implemented. The ECV

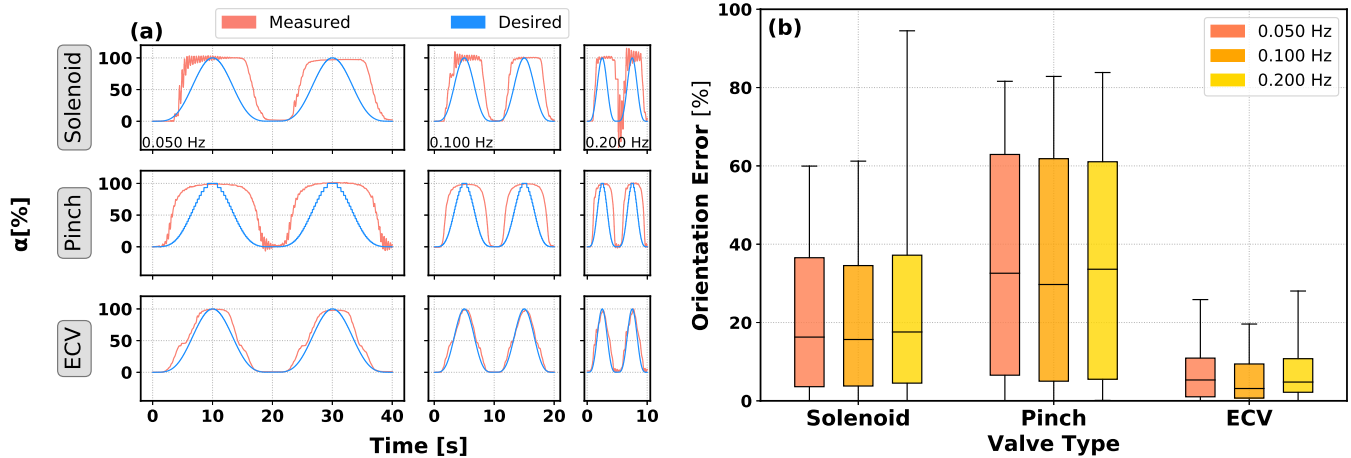


Figure 12. (a) HydroJet capsule bending angle ( $\alpha$ ) as a result of single jet actuation. The angle has been measured considering the initial orientation (tether and capsule aligned with the gravity vector) as reference ( $0^\circ$ ) and a maximum bending angle of about  $70^\circ$ . (b) Orientation error measured as the difference between the desired and measured bending angle.

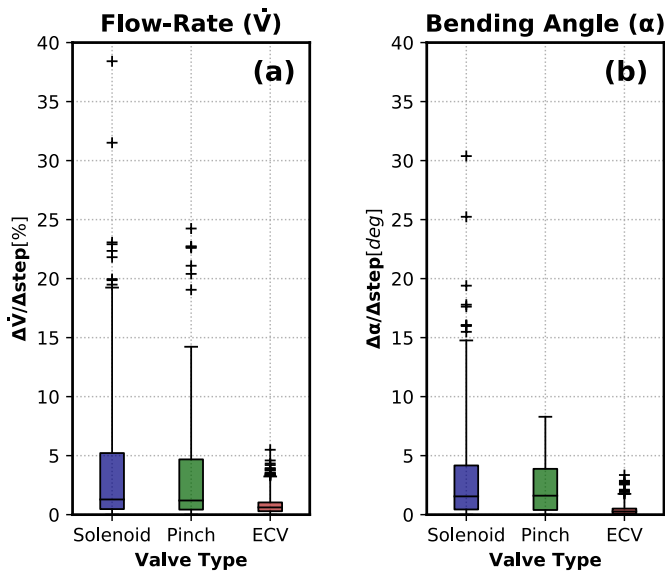


Figure 13. Flow-rate (a) and bending angle (b) fluctuation as a result of opening/closing the each valve one step at a time. Outliers policy:  $3 \cdot IQR$ .

offers a generic platform for application in pneumatic and hydraulic systems where sanitary flow regulation is required (e.g. medical applications). The valve is easy to fabricate thanks to the simple principle of operation which relies on off-the-shelf, machined and 3D printable components, even if the machined parts demand the manufacturing process to be sufficiently accurate. By exploiting a large and adaptable compression profile, increased resolution and linearity may be manufactured into the device; accounting for application specific requirements. To this end, we have presented a device-specific optimization strategy that shows improved linearity when compared to a standard linearly-varying profile, and to commercially available alternative valves. Through increasing the tubing contact area under compression, a significant reduction in plastic deformation (up to about 96% reduction for tube durometer 60A) and its associated influence on flow-rate

(up to 98% for tube durometer 65A) vs valve position was shown across a range of tubing durometers. To demonstrate the significance of these improvements on a real system, an optimized profile ECV was compared with pinch and solenoid valves for controlling the orientation of a water propelled tethered capsule (the HydroJet). A significant overall reduction in error with respect to the commanded behaviour has been shown, with mitigation of oscillatory movements. Ultimately, this allows for suitable open loop control of the orientation of the tip, where the linearity of the ECV allows for close following of the desired signal across frequencies.

The ECV has demonstrated the potential for a new sanitary valve actuation method that could aid in delivering more precise open-loop flow control systems and facilitate development of the next generation of medical soft robots.

## REFERENCES

- [1] T. George Thuruthel, Y. Ansari, E. Falotico, and C. Laschi, "Control Strategies for Soft Robotic Manipulators: A Survey," *Soft Robotics*, no. January, p. soro.2017.0007, 2018. [Online]. Available: <http://online.liebertpub.com/doi/10.1089/soro.2017.0007>
- [2] B. S. Homborg, R. K. Katschmann, M. R. Dogar, and D. Rus, "Haptic Identification of Objects using a Modular Soft Robotic Gripper," *2015 IEEE/Rsj International Conference on Intelligent Robots and Systems*, pp. 1698–1705, 2015.
- [3] E. W. Hawkes, L. H. Blumenschein, J. D. Greer, and A. M. Okamura, "A soft robot that navigates its environment through growth," *Science Robotics*, vol. 2, no. 8, p. eaan3028, 2017. [Online]. Available: <http://robotics.sciencemag.org/lookup/doi/10.1126/scirobotics.aan3028>
- [4] R. F. Shepherd, F. Ilievski, W. Choi, S. A. Morin, A. A. Stokes, A. D. Mazzeo, X. Chen, M. Wang, and G. M. Whitesides, "Multigait soft robot," *Proceedings of the National Academy of Sciences*, vol. 108, no. 51, pp. 20400–20403, 2011. [Online]. Available: <http://www.pnas.org/cgi/doi/10.1073/pnas.1116564108>
- [5] K. C. Galloway, K. P. Becker, B. Phillips, J. Kirby, S. Licht, D. Tchernov, R. J. Wood, and D. F. Gruber, "Soft robotic grippers for biological sampling on deep reefs," *Soft Robotics*, vol. 3, no. 1, pp. 23–33, 2016, pMID: 27625917. [Online]. Available: <https://doi.org/10.1089/soro.2015.0019>
- [6] J. Burgner-Kahrs, D. C. Rucker, and H. Choset, "Continuum robots for medical applications: A survey," *IEEE Transactions on Robotics*, vol. 31, no. 6, pp. 1261–1280, 2015.

- [7] M. Cianchetti, T. Ranzani, G. Gerboni, T. Nanayakkara, K. Althoefer, P. Dasgupta, and A. Menciassi, "Soft Robotics Technologies to Address Shortcomings in Today's Minimally Invasive Surgery: The STIFF-FLOP Approach," *Soft Robotics*, vol. 1, no. 2, pp. 122–131, 2014. [Online]. Available: <http://online.liebertpub.com/doi/abs/10.1089/soro.2014.0001>
- [8] F. Campisano, F. Gramuglia, I. R. Dawson, C. T. Lyne, M. L. Izmaylov, S. Misra, E. D. Momi, D. R. Morgan, K. L. Obstein, and P. Valdastrì, "Gastric cancer screening in low-income countries: System design, fabrication, and analysis for an ultralow-cost endoscopy procedure," *IEEE Robotics Automation Magazine*, vol. 24, no. 2, pp. 73–81, June 2017.
- [9] E. T. Roche, M. A. Horvath, I. Wamala, A. Alazmani, S. E. Song, W. Whyte, Z. Machaidze, N. V. Vasilyev, D. J. Mooney, F. A. Pigula, and C. J. Walsh, "Soft Robotic Sleeve Restores Heart Function," *Science Translational Medicine*, vol. 9, no. 373, p. eaaf3925, 2017.
- [10] M. Wehner, Y. L. Park, C. Walsh, R. Nagpal, R. J. Wood, T. Moore, and E. Goldfield, "Experimental characterization of components for active soft orthotics," *Proceedings of the IEEE RAS and EMBS International Conference on Biomedical Robotics and Biomechanics*, pp. 1586–1592, 2012.
- [11] V. R. Muthusamy and A. S. Ross, "Sa1068 Economic Burden of Emergent Practices of Duodenoscopes Reprocessing and Surveillance: Balancing Risk- and Cost-Containment," *Gastrointestinal Endoscopy*, vol. 87, no. 6, Supplement, pp. AB167 – AB168, 2018. [Online]. Available: <http://www.sciencedirect.com/science/article/pii/S0016510718316948>
- [12] M. M. Schmauch, S. R. Mishra, B. A. Evans, O. D. Velez, and J. B. Tracy, "Chained Iron Microparticles for Directionally Controlled Actuation of Soft Robots," *ACS Applied Materials and Interfaces*, vol. 9, no. 13, pp. 11 895–11 901, 2017.
- [13] K. W. Oh, R. Rong, and C. H. Ahn, "Miniaturization of pinch-type valves and pumps for practical micro total analysis system integration," *Journal of Micromechanics and Microengineering*, vol. 15, no. 12, pp. 2449–2455, 2005.
- [14] G. J. Peek, K. Wong, C. Morrison, H. M. Killer, and R. K. Firmin, "Tubing failure during prolonged roller pump use: A laboratory study," *Perfusion*, vol. 14, no. 6, pp. 443–452, 1999.
- [15] M. Liermann, "Active Pneumatic Pulsation Damper for Peristaltic Pump Flow Loops," in *BATH/ASME 2016 Symposium on Fluid Power and Motion Control*. ASME, sep 2016, p. V001T01A005.
- [16] R. Caprara, K. L. Obstein, G. Scozzarro, C. Di Natali, M. Beccani, D. R. Morgan, and P. Valdastrì, "A platform for gastric cancer screening in low- and middle-income countries." *IEEE Transactions on Biomedical Engineering*, vol. 62, no. 5, pp. 1324–1332, 2015.
- [17] F. Campisano, F. Gramuglia, I. R. Dawson, K. L. Obstein, S. Misra, E. De Momi, and P. Valdastrì, "Water Jet Actuation for Ultra-low Cost Endoscopy: Characterization of Miniature Nozzles Fabricated by Rapid Prototyping," *Procedia Engineering*, vol. 168, pp. 388–391, 2016. [Online]. Available: <http://dx.doi.org/10.1016/j.proeng.2016.11.147>
- [18] NIH (The National Institute of Diabetes and Digestive and Kidney Diseases), "Upper GI Endoscopy." [Online]. Available: <https://www.niddk.nih.gov/health-information/diagnostic-tests/upper-gi-endoscopy>



**Simone Calò** (S'17) received a B.S. and a M.S. degree in Biomedical Engineering from Politecnico di Milano, Milan, Italy, in 2013 and 2016, respectively. In 2016 he began his Ph.D. studies in School of Electronic and Electrical Engineering at the University of Leeds, Leeds, UK. He is a Member of the Science and Technology of Robotics in Medicine (STORM) Laboratory UK where he is primarily involved in the development of low-cost technologies for gastric cancer screening.



identifying tissue disease.

**James H. Chandler** received the M.Eng degree in Mechanical engineering and Ph.D. degree in Surgical Technologies from University of Leeds, Leeds, UK, in 2011 and 2016 respectively. He is currently a Research Fellow in the Institute of Robotics, Autonomous Systems and Sensing, School of Electronic and Electrical Engineering, University of Leeds, Leeds, UK working on low-cost endoscopic technology for gastric cancer screening. His research interests include soft robotic systems for surgery, tissue mechanics and sensing technology for



**Federico Campisano** (S'14) received a B.S. in electronic engineering and a M.S. degree in Biomedical Engineering from Politecnico di Milano, Milan, Italy, in 2011 and 2014, respectively. Since then, he has been working toward the Ph.D. degree in mechanical engineering at Vanderbilt University, Nashville, TN, USA. He is a Member of the Science and Technology of Robotics in Medicine Laboratory USA, and his research interests include medical robotics, compliant continuum devices and new technologies for tissue palpation.



**Keith L. Obstein** earned his B.S. from Johns Hopkins University Whiting School of Engineering (Baltimore, MD), M.D. from Northwestern University (Chicago, IL), and M.P.H. from Harvard University School of Public Health (Boston, MA). He completed Internal Medicine residency at the Hospital of the University of Pennsylvania (Philadelphia, PA) and Gastroenterology (GI) fellowship at the Brigham and Women's Hospital (Boston, MA). Currently, he is an Associate Professor of Medicine and of Mechanical Engineering at Vanderbilt University (Nashville, TN). He is also the Program Director of the Vanderbilt GI Fellowship training program and Director of the Science and Technology Of Robotics in Medicine (STORM) Lab USA at Vanderbilt. He is an active clinician and conducts research in the areas of New Technologies, Robotics, Device Development, Endoscopic Training, and Healthcare Quality Improvement. Dr. Obstein is a Fellow of the American Society for Gastrointestinal Endoscopy (FASGE), the American College of Gastroenterology (FACG), and the American Gastroenterological Association (AGAF). He is board certified in gastroenterology and serves on the ASGE Recognized Industry Associate (ARIA) task force, the ASGE member engagement and diversity committee, the ACG public relations committee, and is the Continuing Medical Education (CME) special section editor of the journal *Gastroenterology*.



**Pietro Valdastrì** (M'05, SM'13) received a Master's (Hons., Univ. Pisa, 2002) and Ph.D. (Biomed. Eng, SSSA, 2006). He is Professor and Chair in Robotics and Autonomous Systems at University of Leeds and recipient of the Wolfson Research Merit Award from the Royal Society. His research interests are in robotic surgery, robotic endoscopy, design of magnetic mechanisms and medical capsule robots.